An investigation into the influence of geometry on compressed earth building blocks using finite element analysis.

Author Information:

Author Names and Affiliations: Jack Andrew Cottrell, Dr Muhammad Ali, Dr Alireza Tatari, Dr D. Brett Martinson.

Corresponding Author: Jack Andrew Cottrell

Corresponding Author Address: School of Civil Engineering and Surveying, University of Portsmouth, Portland Building, Portland Street, Portsmouth PO1 3AH, United Kingdom

Corresponding Author Email Address: jack.cottrell@port.ac.uk

Highlights:

1. Design and manufacture of a manual compressed earth block machine.
2. Physical and numerical testing of un-stabilised compressed earth blocks with different geometric properties.
3. Development of a macro finite element model for un-stabilised compressed earth blocks utilising a modified Solid65 material model.
4. Accuracy and robustness assessment of the numerical model including sensitivity analysis to account for block imperfections.

Graphical Abstract:

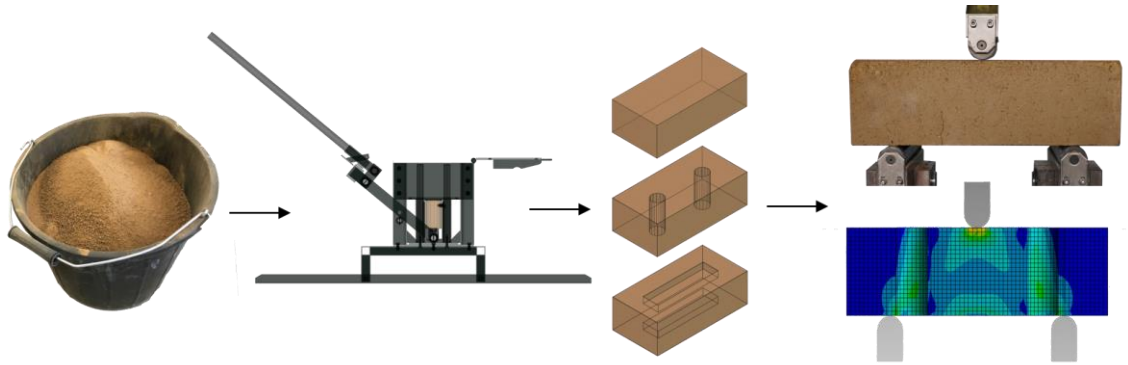

Abstract:

This paper presents a parametric investigation into the influence of geometry on the compressive and flexural strength of un-stabilised compressed earth blocks (CEBs). Three CEBs with dissimilar geometric properties were manufactured and subjected to physical testing and Finite Element Analysis (FEA) using ANSYS Workbench 19.1. The compressive and flexural strength of the CEBs were shown to be dependent on their geometric properties and ranged from 3.74 – 6.73 MPa and 0.63 – 1.31 MPa respectively. A modified Solid65 element command was utilised within the FEA and was shown to successfully replicate the non-linear elasto-plastic behaviour observed in physical testing.

Keywords:

1. Un-stabilised Compressed Earth Blocks
2. CEB Machine
3. Geometric Properties
4. Compressive and Flexural Strength
5. Finite Element Analysis

1.0 - Introduction:

Earth is recognised to be one of the first and most utilised building materials, with evidence suggesting that humans have been shaping and compacting earth to form shelter since 8300 B.C. [1]. It is estimated that more than a third of all humanity lives in a home built of earth [2], with particularly high proportions residing in low-income countries.

The modern-day application of earthen construction may be perceived as inferior to the typical fired brick, concrete and steel construction that dominates much of current architecture. However, the benefits of using earth in construction are widely researched and known to offer a low cost and sustainable building solution with low environmental impact, excellent moisture control, good thermal performance and good acoustic insulation [1–6] .

Unlike traditional methods, such as adobe or rammed earth, the compressed earth block (CEB) is a relatively modern type of earthen construction [7]. The first known CEB machine was invented in the 18th century by French creator Francois Cointeraux, who adapted a wine-press to compact and form earth building blocks [8].

In 1952 the invention of the hand-powered ClNVA-RAM press, designed by engineer Raul Ramirez, revolutionised CEB technology [9]. The development of this low-cost machine enabled small scale production of relatively high-quality earth building blocks which led to an increase in the application of CEB construction. Within the last 40 years, there has appeared a new generation of manual, mechanical and motor-driven CEB machines which has established a genuine market for the production and application of the CEB as a modern building material. Despite the recent developments, there is lack of technical details in the scientific domain as to how manual CEB presses could be designed and operated to produce desired earth blocks, in particular for practitioners in remote areas where mechanised production plants cannot be installed.

Due to the desirable mechanical properties and increased demand, extensive research and development have been carried out to improve the material properties of CEBs. When comparing data from twenty-three studies [10], the compressive strength of un-stabilised CEBs ranged from 0.09 MPa to 5.15 MPa. In contrast, various studies have shown that CEBs can exceed a compressive strength of 20.00 MPa when enhanced with chemical stabilisers such as cement or lime [11–13]. To put this in perspective, the requirements of design strength of bricks and masonry units within the UK

are detailed in British Standard BS EN 1996-1-1:2005 [14,15] where the minimum compressive strength of 10 MPa or 13 MPa is required for two or three-storey dwellings respectively.

The addition of cement or lime has proven successful in increasing the mechanical strength and durability of CEBs. However, the incorporation and associated production of chemical stabilisers such as Portland cement (PC) contributes significantly to anthropogenic CO_2 emissions in the atmosphere [16] and has a significant impact on the cost of production. Therefore, the partial or total replacement of PC is critical to the achievement of sustainable development of infrastructure. It is for this reason that un-stabilised CEBs are the focus of this investigation.

The latest development of CEB machines has seen the incorporation of interchangeable inserts to enable the production of bricks with various shapes and sizes, as shown in **Fig. 1**.

Fig. 1. Different Geometries of Compressed Earth Blocks. Figure derived from [17]

While the investigation into the material properties of CEBs have been extensive and well documented, there has been little investigation into the influence of geometry on the mechanical properties of CEBs. A previous study performed physical testing to investigate the influence of aspect ratio (ratio of specimen height to width) on the compressive strength behaviour of CEBs [18]. The aforementioned study found that the typical aspect ratio for a CEB (between 0.5 – 1.0) obtained the greatest compressive strength, while the most significant reduction in strength was observed in blocks with an aspect ratio between 1.0 - 2.0. In order to develop further understanding of the influence of complex geometry such as those shown in **Fig. 1**, it is necessary to employ finite element analysis.

The utilisation of finite element analysis (FEA) to study the properties of CEBs has been very limited. Of the few studies that have utilised FEA, there has been success in modelling the mechanical behaviour of earthen construction and various approaches have been taken to do so [5,19–24]. A previous study utilised FEA to investigate the interaction between individual interlocking CEB's stacked on top of one another, and was shown to successfully replicate the cracking pattern observed within physical testing [20]. Further studies have utilised FEA to model structural elements such as walls to determine the behaviour of traditional adobe masonry and CEBs under static and seismic loading [19,24]. Generally, the application of FEA has proven successful in determining accurate load-displacement curves, crack patterns, local stresses and deformations.

Until now, the influence of complex block geometry on mechanical properties such as compressive and flexural strength has not been investigated. The purpose of this investigation is to determine the influence of geometry on un-stabilised compressed earth building blocks using a parametric approach that considers both physical testing and finite element analysis. This will be achieved by comparison of three common block types with varying geometry. It is assumed that three shapes studied in this investigation should provide an insight into the effects of geometry on the durability and overall performance of various shapes of CEBs.

2.0 - Materials and Methods:

2.1 – Design and Manufacture of Compressed Earth Block Machine

To facilitate the study, a University of Portsmouth Compressed Earth Block Machine (UoP-CEB machine) was designed and manufactured, as shown in **Fig. 2**. The UoP-CEB has the capability of creating different blocks with interchangeable moulds. During the design development of the UoP-CEB machine, the design of current manual CEB machines, such as the CINVA-Ram, CETA-Ram and Tek-Block [9] were reviewed and developed as described below.

Unlike any other manual CEB machine found in existing literature, the design incorporates a hydraulic ram positioned beneath the baseplate to measure the amount of compaction pressure being applied to the block during compression. Previous studies have shown that the greater compaction pressure during the manufacture, the greater mechanical properties achieved [6]. Due to the importance of compaction pressure [25,26], it is crucial for the operator of the UoP-CEB machine to know the amount of pressure applied to the block so that quality and consistency within the manufacturing process is maintained.

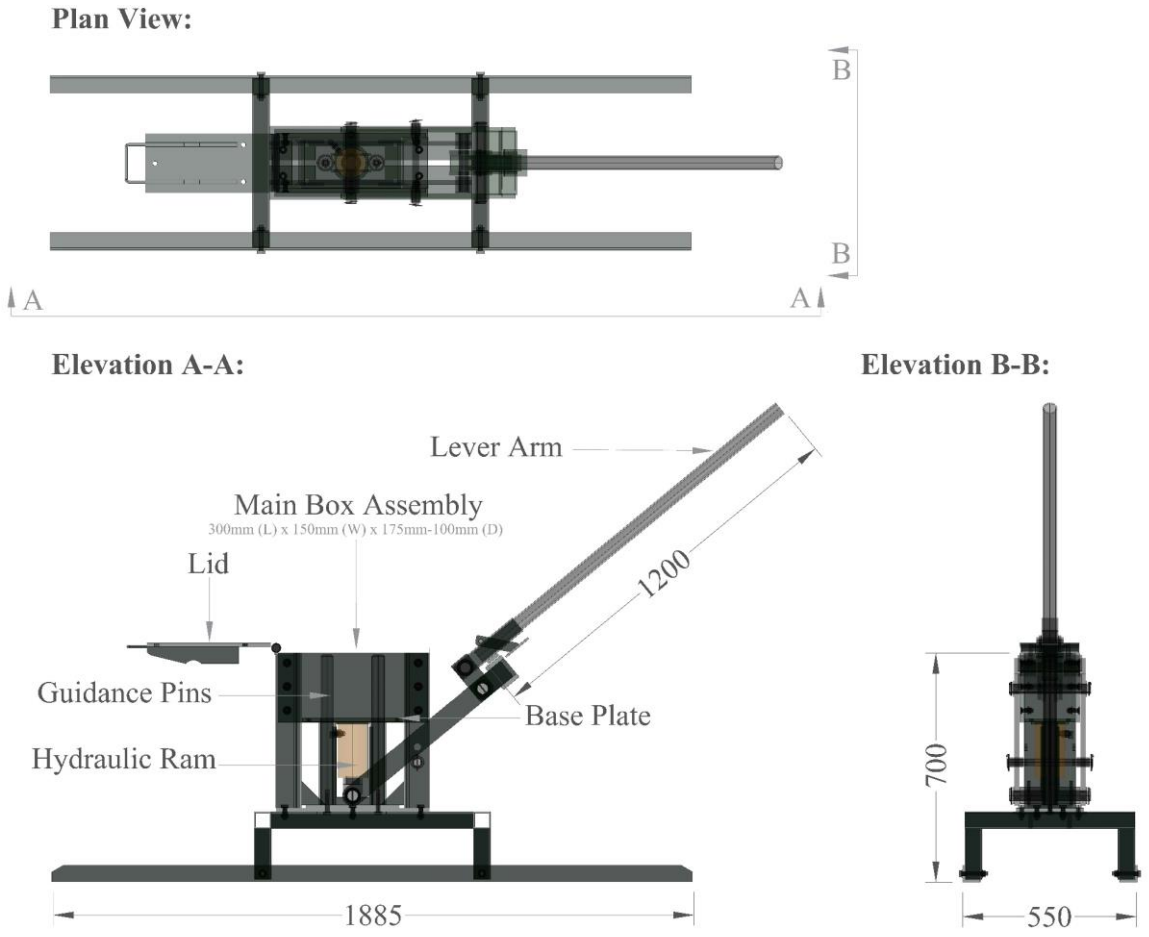

Fig. 2. Drawing of UoP-CEB Machine (50% Transparency to Show Hidden Critical Elements) Drawn in AutoCAD 2019 [27]

The UoP-CEB machine was manufactured out of minimum grade S275 steel and was designed produce a CEB with dimensions 300mm (L) x 150mm (W) x 90-110mm (H). Different inserts can be secured to the baseplate and lid of the main box assembly to form different compressed earth blocks, such as interlocking blocks. The guidance pins in the main box assembly are interchangeable to enable the production of solid blocks or hollow blocks. Hollow blocks feature two 38mm diameter holes passing through the height of the block at 150mm centres. When constructing a wall, hollow blocks to enable vertical reinforcement to be passed through the wall to increase lateral stability and resistance against wind or seismic loading.

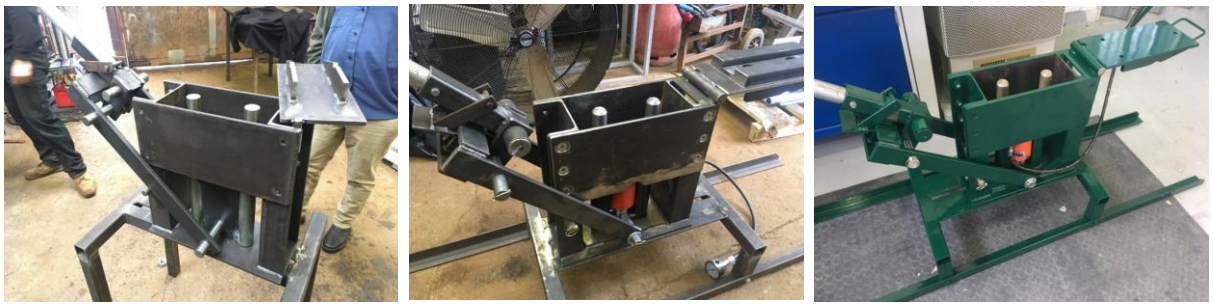

Fig. 3. Design Development of the UoP-CEB Machine

2.2 – Testing and Calibration of Compressed Earth Block Machine

Following the manufacture of the UoP-CEB machine, it was subjected to a series of quantitative and qualitative tests to determine the optimum compaction pressure, safe working limits and optimum material dosage.

2.2.1 – Optimum Compaction Pressure and Safe Working Limits

The hydraulic ram and pressure gauge were calibrated using a known load applied by a Zwick/Roell Z250 250kN Universal testing machine. Equation (1) shows the conversion from the amount of pressure measured on the pressure gauge in PSI (A) to the amount of pressure applied to the block in MPa. This equation considers the calibrated behaviour of the hydraulic ram and pressure gauge.

(1) UoP-CEB Machine Pressure Gauge Conversion:

$$\text{Pressure Applied to Block (MPa)} = \text{P} \times \frac{A_1}{(A_2 \times 145.038)} \times K$$

Pressure Gauge Reading = P (PSI)

Effective Area of Hydraulic Ram, A_1 = 3,318mm^2

Surface Area of Base Plate, A_2 = 45,000mm^2

PSI to MPa Conversion Factor = 145.038

Calibration Constant, K = 0.94

A target pressure was determined following a qualitative assessment of the CEBs produced at different pressures. This assessment was performed through observation such as size of block, number of surface cracks and regularity of compaction. The observations of the Solid Block, Solid Block with Frogs and Hollow block are summarised in **Table 1** and are consistent with previous studies [6].

Table 1
Determination of Optimum Compaction Pressure Through Qualitative Analysis

Observation:	**Pressure Applied to Block (MPa)**			
	0.00 – 0.50	**0.50 – 1.00**	**1.00 – 1.50**	**1.50 – 2.00**
Surface Appearance	▪ Excessive surface cracks, fissures and voids.	▪ Smooth surface finish on sides of block. Few surface cracks observed on top and bottom.	▪ Smooth surface finish on all faces of block.	**Machine operator is unable to manually lower the lever arm without difficulty.**
Uniformity of Compaction	▪ Obvious signs of incomplete compaction across the length, width and depth.	▪ Slight signs of incomplete compaction across the depth of block.	▪ Good uniformity observed across the length, width and depth.	
Geometric Imperfections	▪ Edges and vertices are poorly formed and easily broken with pressure applied by hand.	▪ Edges and vertices exhibit some geometric imperfections at the extremities.	▪ Edges and vertices are well formed and have few geometric imperfections.	

To ensure consistency in the manufacture of the blocks, a target pressure of 1.25 MPa was determined, with an acceptable tolerance of +/-10%. At +1.5 MPa, the physical limitation of the UoP-CEB machine was observed as the operator is unable to lower the lever arm without applying excessive force.

2.2.2 – Optimum Material Dosage

During the manufacture of blocks, the amount of soil was carefully calculated to ensure that the optimum pressure was achieved. The dosage into the UoP-CEB Machine was calculated based on density of the material at optimum moisture content, obtained from the proctor test, as shown in equation (2).

(2) UoP-CEB Machine Optimum Material Dosage:

$$\text{Dosage } (kg) = \text{Density at OMC } (kg/m^3) \times \text{Volume of Compressed Block } (m^3)$$

As a force is applied to the lever, the position of the roller mechanism is transferred over the top dead centre of the main box assembly. The two arms that connect the roller mechanism to the base plate cause the base plate to rise by 75mm and consequently the volume within main box assembly is reduced from 7.65×10^6 mm^3 to 4.5×10^6 mm^3 as illustrated in **Fig. 4**.

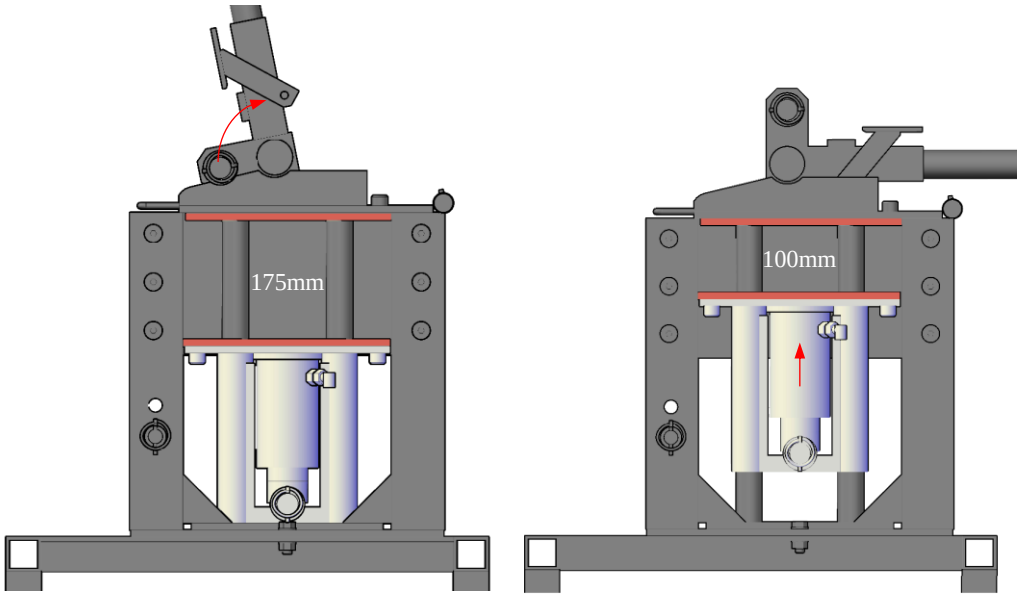

Fig. 4. A diagram showing reduction in volume of main box assembly during compression drawn in AutoCAD [27].

2.3 – Manufacture of Blocks

2.3.1 - Properties of the Material

For this study, a loessic soil, also known as brickearth found in Kent (south east of England) was used. Kent Brick Earth (KBE) can be described as an orangey-brown slightly sandy very silty CLAY with occasional gravel fragments. A particle size distribution test was performed using a Mastersizer 3000 particle size analyser [28] and the KBE was shown to have approximately 22% clay, 56% silt and 22% sand content.

Approximately 20% additional non-uniform particle size marine sand by weight was incorporated into the CEB mix to conform with the recommended sand content of between 25-50% [29]. The additional sand content prevents the formation of shrinkage cracks as the blocks lose moisture content during the drying phase. The material properties of the KBE and KBE with marine sand, including the particle size distribution to BS1377-2:1990 [30], can be seen in **Table 2**.

Table 2
Properties of Kent Brick Earth

Properties	Soil Type	
	Kent Brick Earth	**Kent Brick Earth with Marine Sand**
Proctor Test		
Optimum Moisture Content (%)	13.0	12.5
Maximum Dry Density (Mg/m^3)	1.95	2.16
Atterberg Limits		
Liquid Limit LL (%)	34.1	26.3
Plastic Limit PL (%)	16.6	15.3
Plastic Index PI	17.5	10.9
Soil Classification		
Unified Soil Classification System	CL	CL
Particle Size Distribution		
Gravel (> 2.0mm) (%)	0.0	0.00
Sand (2.0 – 0.063mm) (%)	22.1	38.8
Silt (0.063 – 0.002mm) (%)	55.9	50.1
Clay (<0.002mm) (%)	22.0	11.1

During the manufacture of the blocks, the KBE and marine sand was mixed for 5 minutes at 50 revolutions per minute using a CreteAngle LE standard duty forced action pan mixer [31]. After this time, a consistent mix was observed and the calculated dosage was measured and placed into the CEB machine for compaction.

2.3.2 – Compressed Earth Block Geometry

To investigate the influence of geometry, three different block types were manufactured using the UoP-CEB machine. As outlined in **Table 3**, Six specimens of each block type were manufactured; three replicates of each geometry were tested in compression and 3-point bending respectively.

Table 3
Block Geometry

Block Geometry	Sample Reference	Diagram	Target Mass (g)		Target Moisture Content (%)
			Wet Block	Dry Block	
Solid Block	1A 1B 1C 1D 1E 1F	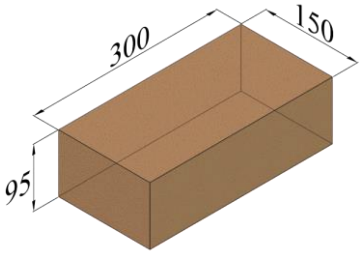	9200	8215	12
Solid Block with Frogs	2A 2B 2C 2D 2E 2F	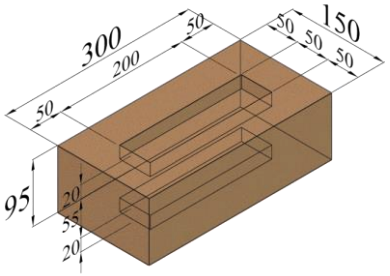	8400	7500	12
Hollow Block	3A 3B 3C 3D 3E 3F	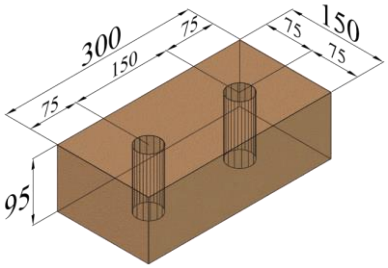	8750	7815	12

Samples A-C were tested in compression and samples D – F were tested in 3-point bending.

2.3.3 – Block Drying

The compressed earth blocks were dried at 30 ^{o}C in a Genlab MINO/100 oven [32] to replicate sun-drying conditions experienced within tropical regions. The blocks were re-weighed throughout the week following the procedure detailed in BS 1377-2: 1990 [30] until a consistent weight was observed +/- 0.01 g indicating that the block was fully dry. Once dried, the compressed earth block exhibited a brittle nature, similar to that of a low strength concrete or breeze block. Prior to testing, the dried blocks were re-weighed and measured.

2.4 – Physical Testing

2.4.1 – Compressive Strength Test

Three replicates of each block type were tested in compression using a Losenhausen 1000 kN universal testing machine.

The compressive strength tests were conducted in accordance with BS EN 772-1 [33]. As per BS EN 772-1, part 7.2.3, masonry units with frogs are to be tested without removing or filling the frogs on the condition that they are assessed to have a net loaded area of more than 35 % of the bed face. The net loaded area of the Solid Block with Frogs was calculated to be 78%, so the frogs were not removed or filled. A 10mm steel plate was positioned on top and beneath the sample to ensure that the load was distributed evenly across the sample.

The load was applied at a rate of 0.05 MPa/s, as per table 02 of BS EN 772-1, until the block failed. The deformation was measured and recorded by gauges built into the Losenhausen 1000 kN universal testing machine. The load at which the block failed was recorded and maximum compressive stress was calculated.

Fig. 5. Compressive Testing of Block Type 1 Before (LHS) and After (RHS) Failure

2.4.2 – 3-Point Bending Test

The deformation was measured and recorded by gauges built into the Zwick/Roell Z250. The use of an external strain gauge on the underside of the slab was not applied due to the risk of the sample failing and causing damage to the gauge. The load at which the block failed was recorded and flexural strength calculated as per BS EN 12390-5 Formula A.2. By obtaining the flexural strength, it was possible to determine the uniaxial tensile stress from existing empirical relationships observed within low strength concrete [41].

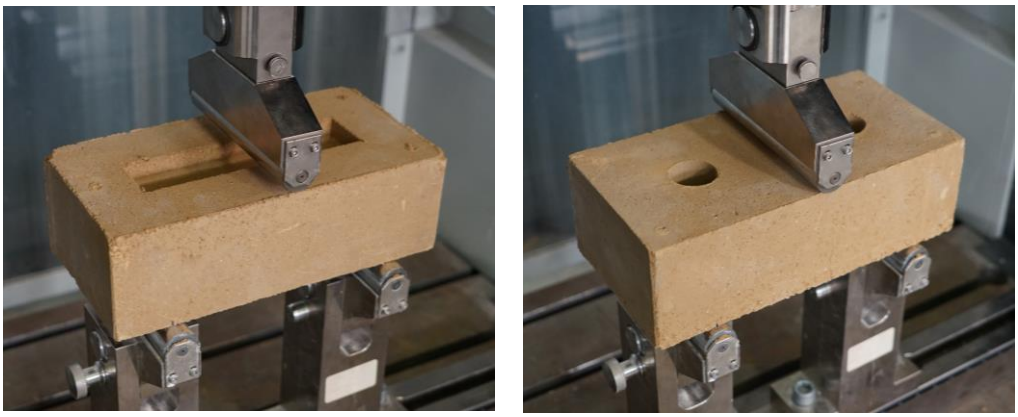

Fig. 6. 3-Point Bending Tests of Block Type 2 (LHS) and Type 3 (RHS)

2.4.3 – Statistical Analysis

To assess the statistical significance of the results obtained from physical testing, statistical analysis (ANOVA with Tukey pairwise comparison) was undertaken with Minitab 17.3.1 [34]. Within the results, statistically significant differences are indicated by different letters (A, B, C) at p-value < 0.005.

2.5 – Numerical Modelling

ANSYS Workbench 19.1 [35] was utilised to investigate the failure mechanism of the CEBs and provide a comparison with the results obtained from physical testing.

Following a rigorous review of existing material models, it was apparent that a non-linear material model for compressed earth was not available. Therefore, the Mechanical ANSYS Parametric Design Language (APDL) was utilised to create a modified element command that could be used to model compressed earth based on the results obtained from physical testing. During physical testing, the CEBs exhibited brittle behaviour similar to that of low strength concrete which influenced the decision to utilise a Solid65 element as the basis of the Mechanical APDL command. The Solid65 element has proven successful in modelling both reinforced and unreinforced concrete, as well as various permutations of masonry construction and individual masonry units [36–41]. The Solid 65 element is defined by eight nodes and has three degrees of freedom at each node; translations in the nodal x, y, and z directions. The Solid65 element is capable of non-linear analysis and demonstrates both cracking in tension and crushing in compression.

The average compressive stress/strain relationship obtained from physical testing of the solid block specimens (1A, 1B and 1C) is shown in **Fig 7**. The results were condensed into five data points, as highlighted in red, from which tabulated data was entered into the Solid65 element command to define the material property. This material property was utilised to model all three types of block.

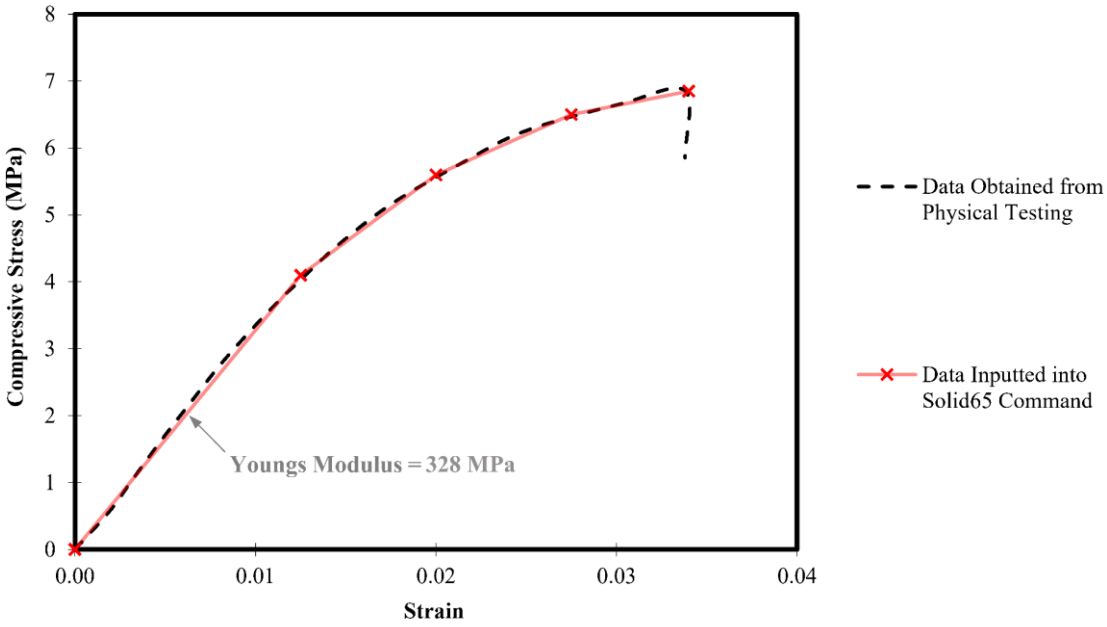

Fig. 7. Data Inputted into Solid65 Command

As the relationship between compressive and flexural strength was known, it was possible to determine the uniaxial tensile stress from existing empirical relationships observed within low strength concrete [42]. A value of 0.70 MPa was considered as the uniaxial tensile stress and was included in the modified Solid65 element command. A summary of the material properties considered within the FEA are detailed in **Table 4** and are within the range of values used within previous studies

[5,20,24,36,45]. The boundary conditions and rate of loading were modelled to replicate the conditions applied in physical testing, as detailed in section 2.4.1 and 2.4.2. The mesh size and step control were determined following an iterative and thorough sequence of sensitivity analysis.

Table 4
Mechanical Properties of Compressed Earth Blocks applied to FEA Model

Mechanical Properties	Value
Young's modulus, E (MPa)	328
Poisson's ratio, ν	0.2
Uniaxial crushing stress, σ_c (MPa)	6.85
Uniaxial tensile cracking stress, σ_t (MPa)	0.7
Shear transfer coefficients for an open crack, βt	0.1
Shear transfer coefficients for a closed crack, βc	0.1
Multilinear isotropic hardening	See figure 7

2.5.1 – Sensitivity Analysis (Mesh Size)

Due to the numerical size limitations associated with the academic license of ANSYS Workbench 19.1, the size of the mesh was often restricted. As shown in **Fig. 8** a sensitivity analysis was performed to determine the influence of the mesh size to ensure that the numerical limitation did not adversely affect the results of the analysis. A mesh size of 5.0mm x 5.0mm was utilised throughout the modelling to ensure acceptable accuracy.

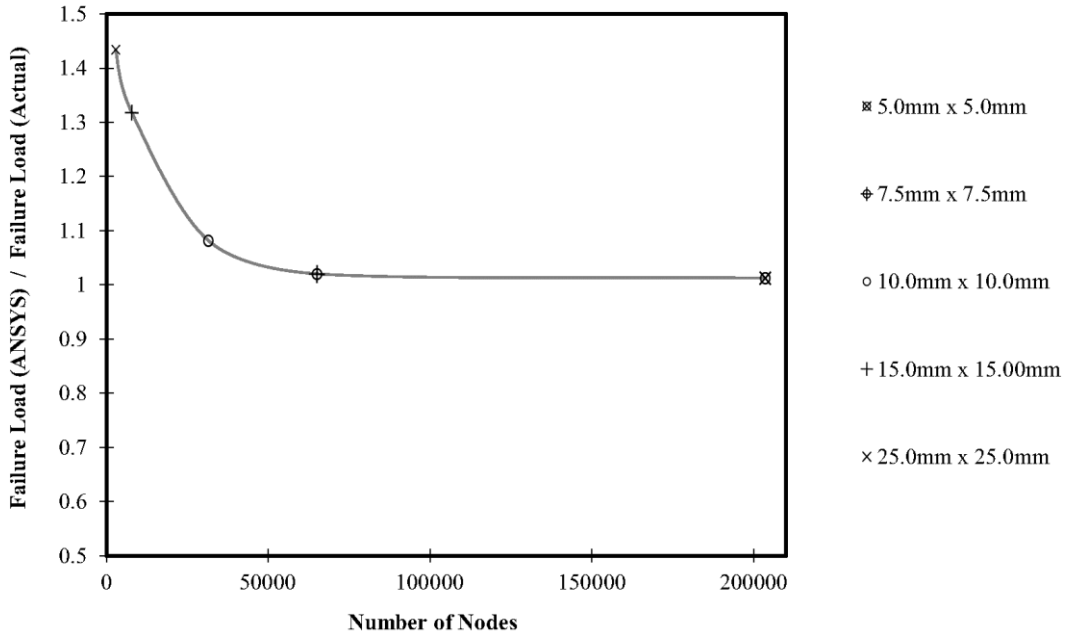

Fig. 8. ANSYS Sensitivity Analysis to Determine Optimum Mesh Size

2.5.2 – Sensitivity Analysis (Damage)

During the manufacture of the blocks, geometric imperfections were observed on the edges and vertices of each block. A sensitivity analysis was performed to determine the influence of damage on the numerical model. As shown in **Fig. 9** the influence of damage was modelled using a 2.5 – 10mm chamfer applied to each edge along the length of the block. The compression and 3-point bending tests were simulated with each of the damage scenarios to determine the influence on compressive and flexural strength. It was observed that damage had a greater influence on flexural strength, with over a 10% reduction in strength with a 10.0mm chamfer.

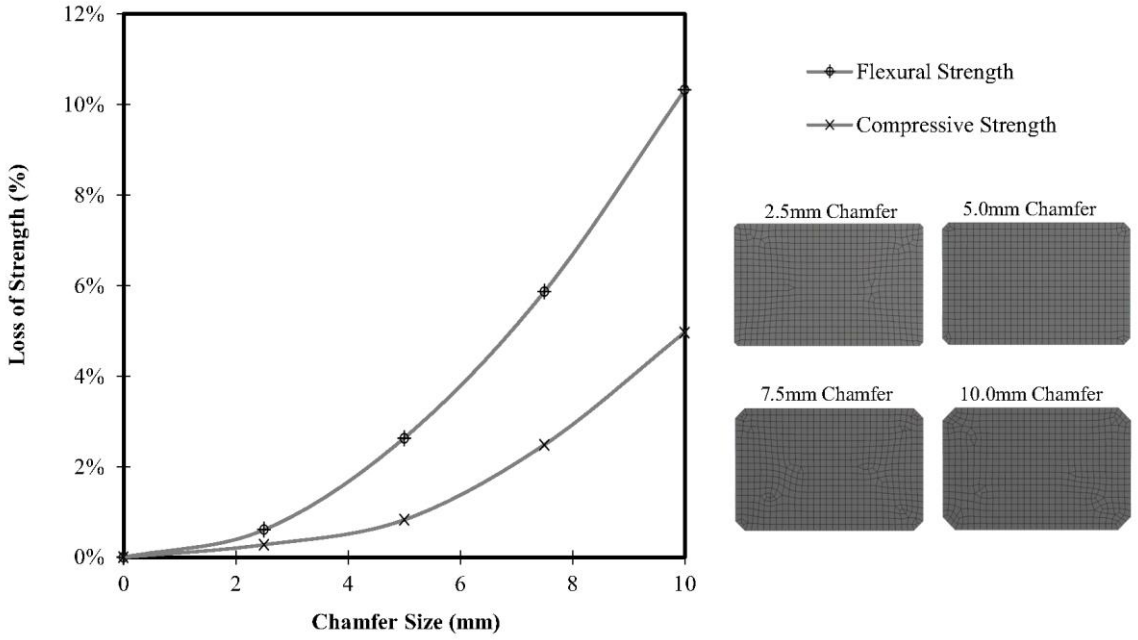

Fig. 9. ANSYS Sensitivity Analysis to Determine Influence of Damage

3.0 - Results:

3.1 – Physical Characteristics of CEBs

The pressure applied during manufacture, mean dry density and mean dry mass of the three block types are presented in **Table 5**.

Table 5
Properties of Compressed Earth Blocks

Block Geometry	Pressure Applied During Manufacture (MPa)	Mean Dry Density (kg/m^3)	Mean Dry Mass (g)
Solid Block	1.22 ± 0.04^{B}	1911.49 ± 3.73^{B}	8171.63 ± 15.93^{A}
Solid Block with Frog	1.29 ± 0.02^{A}	1919.83 ± 2.91^{A}	7439.33 ± 11.27^{B}
Hollow Block	1.21 ± 0.02^{B}	1912.46 ± 6.08^{B}	7774.43 ± 24.70^{C}

Values represent mean ± standard deviation (σ). Results with different letters (A, B, C) indicate values are significantly different from each other at p-value < 0.005.

As shown **Table 5**, in the pressure applied during manufacture was within the target range of 1.25 MPa +/- 10%. As highlighted by the Tukey pairwise comparison, the solid block with frogs was subjected to a slighter higher compaction pressure which resulted in a slightly higher dry density when compared to the solid block and hollow block. The correlation between higher compaction pressure resulting in higher density is consistent with previous studies [6,25,26].

The mean dry density of samples range between 1911.49– 1919.83kg/m^3 which represents a percentage difference of 0.43%. The relatively consistent density can be attributed to the precise method of determining the material dosage and reduces the influence of density on the mechanical properties of the samples. The dry mass of each block is significantly different due to the variation in volume of each geometry type.

As can be seen from **Fig. 10** (a), when tested in compression, the samples exhibited a stress strain relationship similar to that observed in low strength concrete [42]. A region of linear elastic behaviour was present within each of the samples at a deformation of between 0.00 – 2.00mm, or 0.00 – 2.11% strain. The initial linear region transitioned through a parabolic curve into a crushing region where the load remained constant but the deformation continued for approximately 0.50mm or 0.53% strain. During the crushing region, significant cracking was observed on the external faces of the blocks. Due to the brittle nature of the CEB, once the block had reached its failure load it did not demonstrate any residual strength, with a sudden and significant reduction in load capacity.

The specimens also displayed concrete-like behaviour when subjected to the 3-point bending test. As shown in **Fig. 10** (b), the samples demonstrated a linear elastic behaviour until failure which occurred suddenly. Prior to the failure, there was no evidence of cracking on the outer surfaces of the blocks.

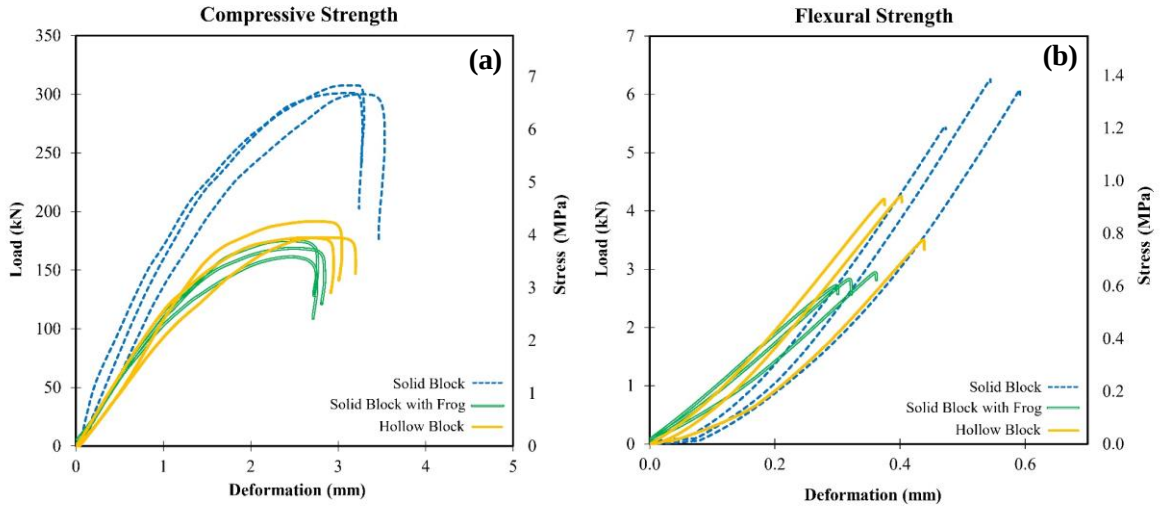

Fig. 10. Results from Physical Testing: Compression (a), 3-Point Bending (b)

The observed relationship between flexural strength and compressive strength of the CEB is consistent with the relationship found within low strength concrete [42]. On average, the compressive strength was approximately 5 times greater than the flexural strength of corresponding block type.

Table 6 summarises the results obtained from physical testing. The solid block exhibited the greatest compressive and flexural strength, followed by the hollow block and lastly the solid block with frog achieved the lowest compressive and flexural strength. The solid block exhibited a 66% greater compressive strength and 48% greater flexural strength in comparison with the hollow block. Similarly, the solid block exhibited an 80% greater compressive strength and 109% greater flexural strength in comparison to the solid block with frogs.

Table 6
Results from Physical Testing

Block Geometry	Test	Experimental Results			
		Mean Failure Load (kN)	Mean Failure Deformation (mm)	Mean Failure Stress (MPa)	Mean Failure Strain (%)
Solid Block	Compression	302.96 ± 3.36	3.20 ± 0.05	6.73 ± 0.07	3.36 ± 0.05
	3-Point Bending	5.93 ± 0.35	0.54 ± 0.05	1.31 ± 0.08	0.56 ± 0.05
Solid Block with Frogs	Compression	168.42 ± 5.67	2.46 ± 0.04	3.74 ± 0.13	2.59 ± 0.04
	3-Point Bending	2.83 ± 0.09	0.33 ± 0.03	0.63 ± 0.02	0.34 ± 0.03
Hollow Block	Compression	182.42 ± 6.49	2.74 ± 0.07	4.05 ± 0.14	2.88 ± 0.07
	3-Point Bending	3.98 ± 0.34	0.40 ± 0.03	0.88 ± 0.08	0.43 ± 0.03

Values represent mean ± standard deviation (σ).

Fig. 11 illustrates the results from physical testing and highlights significant differences within the data at p value < 0.005. As shown, when compared to the other block types, the solid block demonstrates significantly higher values of stress and strain when tested in compression and 3-point bending. There are partial significant differences between the solid block with frogs and hollow block, with the hollow block achieving a higher average stress and strain when testing in compression and 3-point bending. This variance can only be attributed to the geometric differences between the blocks as the material, density and manufacture processes are considered equivalent.

It is recognised that the compressive strength of the solid block is relatively high, with the average compressive strength achieving 6.73 MPa. By comparison, a quantitative assessment of existing literature found that the compressive strength of un-stabilised CEBs ranged from 0.09 MPa to 5.15 MPa [10]. The relatively high compressive strength achieved may be attributed to a series of control measures considered in the manufacture of the blocks, such as mix design, water content, material dosage and compaction pressure, all of which were based on guidance obtained within existing literature [6,10,18,25,26,43,44].

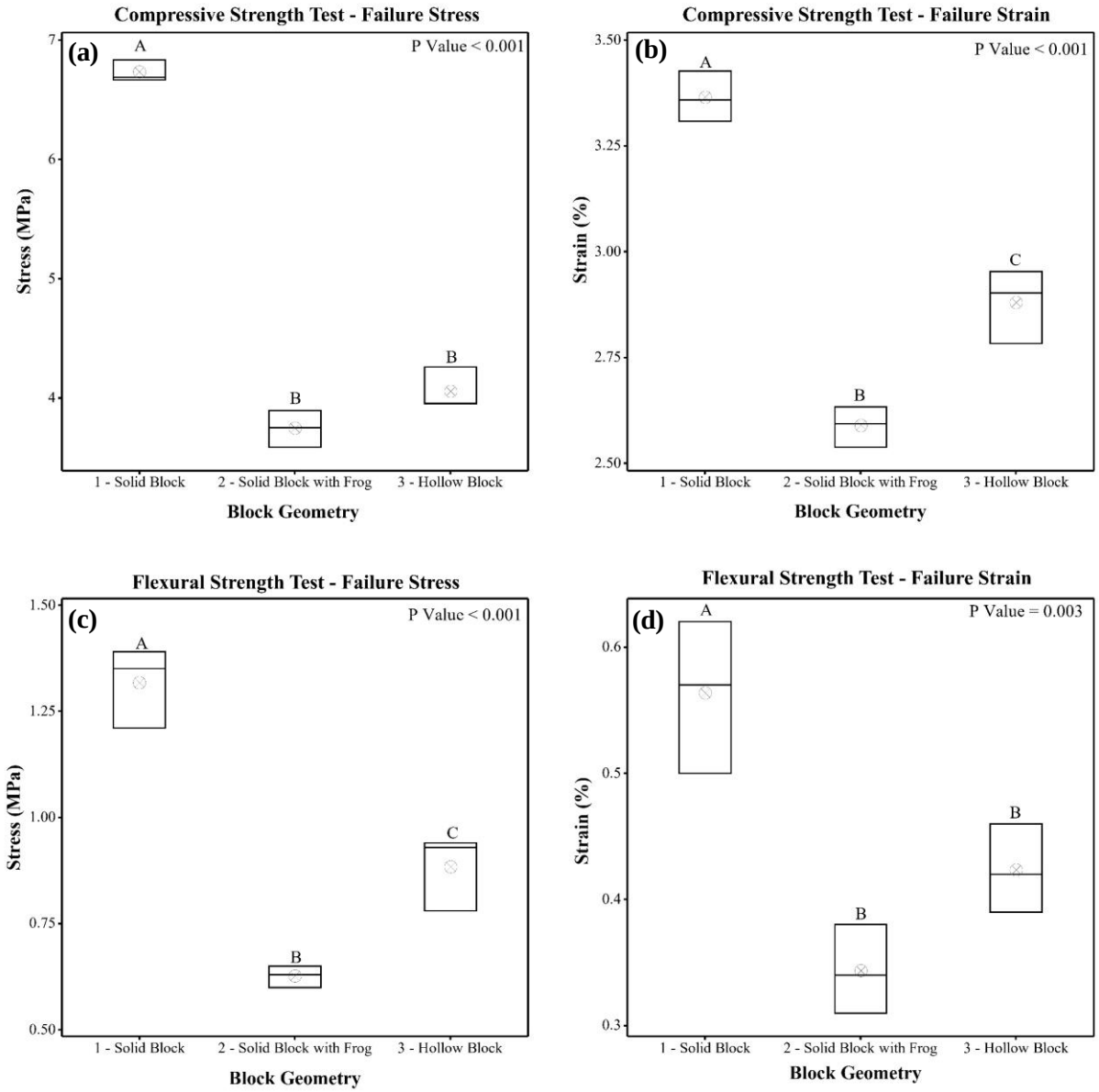

Fig. 11. Box Plot showing (a) compressive strength failure stress, (b) compression testing failure strain, (c) flexural testing failure stress and (d) flexural testing failure strain.

When considering the geometric properties of the blocks, it is reasonable to forecast the outcome of the physical testing. As shown in **Fig. 12** When considering compressive strength, it can be seen that the solid block has 29% and 25% greater surface area that is effective in transferring the load through the sample when compared to the solid block with frog and hollow block respectively. Furthermore, the solid block has a 39% and 34% greater cross-sectional area that is effective in providing resistance to flexural stress when compared to the solid block with frog and hollow block respectively. In order to develop further understanding, it was necessary to employ a FEA to predict the failure mechanism of each type of block.

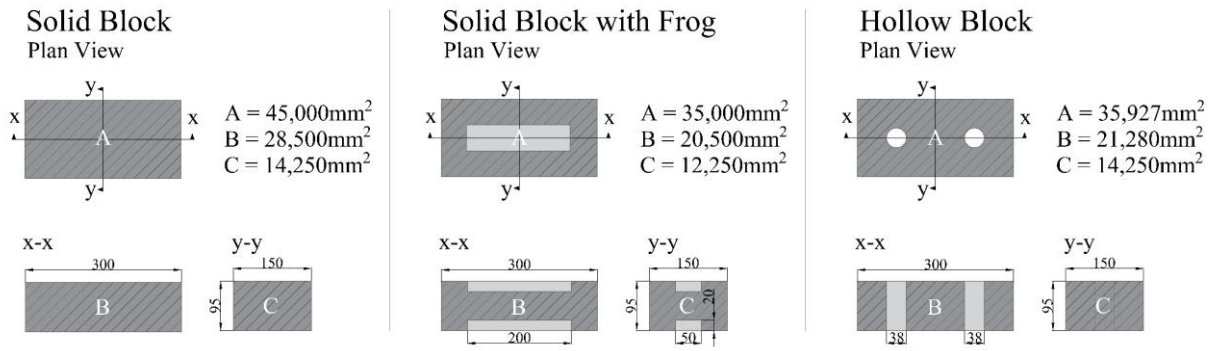

Fig. 12. Cross Sectional Geometric Properties of Blocks

3.2 – Numerical Modelling

The FEA successfully modelled the elasto-plastic nonlinear behaviour of the three block types and the failure point was clearly identified by a sudden large deflection, typical of an elasto-plastic model. The results of the finite element analysis are plotted against the average results from physical testing in **Fig. 13**. As shown, the behaviour of each block type relative to one another is represented in both the physical testing and the numerical modelling.

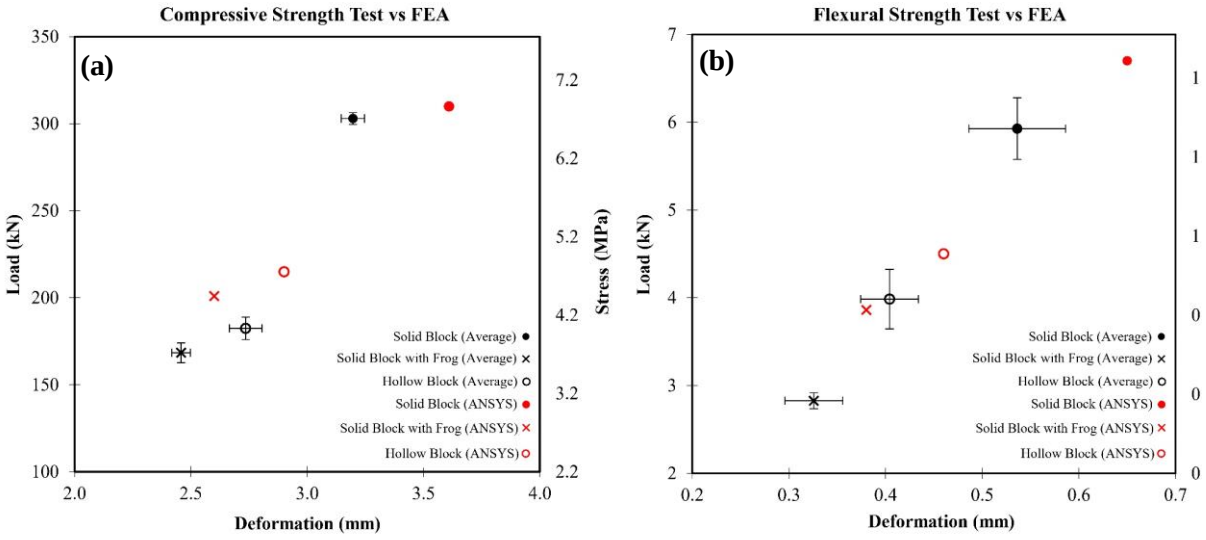

Fig. 13. Results from ANSYS Finite Element Analysis vs Physical Testing: Compression (a), 3-Point Bending (b).

Average results represent mean ± standard error of the mean (n = 3).

As highlighted in **Table 7**, when subjected to compressive strength testing, the numerical model was shown to overestimate the calculated stress by an average of 13.2% and overestimate the calculated strain by an average of 8.2% at point of failure. The most accurate result was obtained for the Solid Block, which calculated the maximum stress within 2.32% of the result obtained from physical testing. The relative accuracy of this analysis was anticipated due to the use of the physical testing data of the solid block for the modified Solid65 element command.

When subjected to the 3-point bending test the numerical model was shown to overestimate the calculated stress by an average of 20.7% and overestimate the calculated strain by an average of 17.2% at point of failure. The finite element analysis successfully determined the relative difference in compressive and flexural strength between the samples.

Table 7
Summary of Results, Physical Testing vs Numerical Modelling

Block Geometry	Test	Experimental Results		Numerical Results		Experimental vs Numerical	
		Mean Failure Stress (MPa)	Mean Failure Strain (%)	Failure Stress (MPa)	Failure Strain (%)	Failure Stress Percentage Difference (%)	Failure Strain Percentage Difference (%)
Solid Block	Compression	6.73	3.36	6.89	3.80	+ 2.32	+ 12.93
	3-Point Bending	1.31	0.56	1.48	0.68	+ 13.05	+ 21.23
Solid Block with Frogs	Compression	3.74	2.59	4.47	2.74	+ 19.35	+ 5.76
	3-Point Bending	0.63	0.34	0.85	0.40	+ 36.19	+ 16.65
Hollow Block	Compression	4.05	2.88	4.78	3.05	+ 17.86	+ 6.02
	3-Point Bending	0.88	0.43	1.00	0.48	+ 12.93	+ 13.82

Previous studies that utilised FEA to investigate the properties of earthen construction have reported qualitative comparisons between experimental and numerical results, such as “satisfactory agreement” or “good correspondence” [5,20,24,36,45]. However, there are limited studies that have reported the percentage variation in the experimental and numerical modelling results. Moreover, there is a lack of justification for the variation in the findings.

There are a number of factors that are considered to influence the marginal variation between the experimental and numerical results. The sensitivity analysis demonstrated the influence of damage on a sample. It is recognised that a 10mm chamfer, equivalent to a 1.83% loss of volume can reduce the compressive and flexural strength as much as 5% and 11% respectively. Considering the potential for imperfection within the physical testing and the expected variation of the natural material, the results obtained from computer modelling may be considered as a theoretical maximum based on perfect conditions.

The failure mechanism of each specimen was examined using various stress tools as illustrated in **Fig. 14**. The stress tools enabled the models to be probed to identify regions of high stress concentration and proved successful in identifying regions of failure which were observed in physical testing.

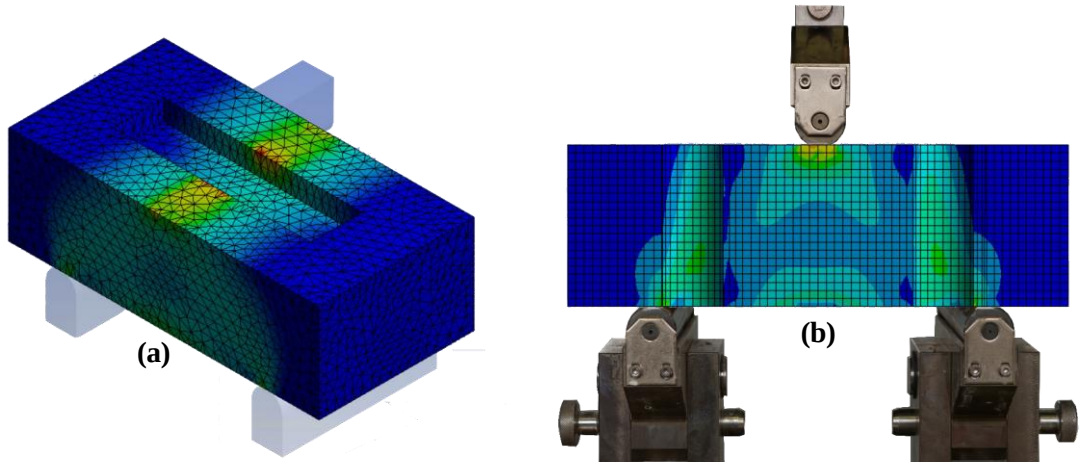

Fig. 14. Stress Distribution during 3-point bending test of Solid Block with Frog (a) and Hollow Block (b) shown in cross section.

The deformation of each sample was also analysed utilising capped isosurfaces, which hide elements that are below or above a specific value of stress, indicating the physical damage within a sample. **Fig. 15** displays the capped isosurfaces for the Solid block following the compressive strength test. As can be seen, the regions of failure are clearly identifiable and correspond to the observations made during physical testing. These findings are similar to previous studies which have utilised ABAQUS [20], DIANA [45] and LY-DYNA [24,46] FEA software packages to successfully replicate stress concentrations and cracking pattern within earth construction. This demonstrates the successful application of a modified Solid65 element command within ANSYS Workbench 19.1 [35] to model the elasto-plastic nonlinear behaviour of un-stabilised CEBs.

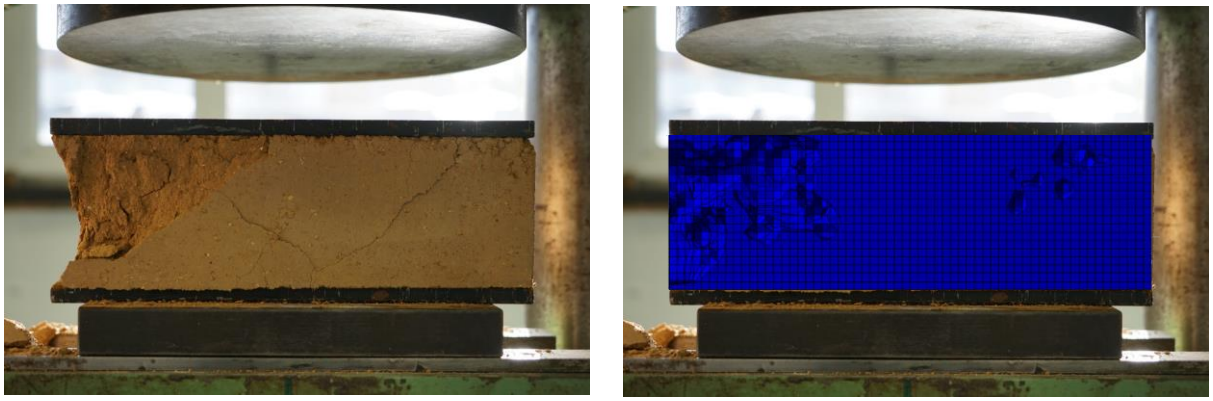

Fig. 15. Total Deformation (Capped Isosurface)

4.0 - Conclusions:

The results obtained from the physical testing and numerical modelling demonstrate the influence of geometry on the compressive strength and flexural strength of un-stabilised compressed earth building blocks. The important conclusions emerging from this study are:

- The geometry of un-stabilised CEBs has a significant influence on its compressive and flexural strength and should be a primary consideration when selecting or developing new compressed earth blocks.
- The Solid Block exhibited the greatest compressive and flexural strength at 6.73 MPa and 1.31 MPa respectively, whilst the Solid Block with Frogs exhibited the lowest compressive and flexural strength at 3.74 MPa and 0.63 MPa respectively.
- Finite Element Analysis within ANSYS Workbench 19.1 can be utilised in conjunction with a modified Solid65 element command to successfully modelled the non-linear elasto-plastic behaviour observed in physical testing.
- Finite Element Analysis within ANSYS Workbench 19.1 can be utilised in conjunction with a modified Solid65 element command to successfully identifies regions of stress concentrations.
- Robust/controlled production methods for un-stabilised CEB using a manual press can lead to superior building blocks.
- Influence of damage on un-stabilised CEBs is significant and must be considered when developing a finite element analysis to model the properties of compressed earth.

Following the successful development of a Solid65 element code to model un-stabilised CEBs, further investigation into the influence of damage and localised defects is required to reduce the variation between physical testing and numerical modelling. Moreover, the application of FEA to assess the influence of stabilisers, admixtures and a variety of fibre reinforcement is recommended to promote further development of the mechanical properties of CEBs to provide a superior low-cost building material.

List of Abbreviations:

- **APDL** – ANSYS Parametric Design Language
- **CEB(s)** – Compressed Earth Block(s)
- **FEA –** Finite Element Analysis
- **KBE –** Kent Brick Earth
- **OMC –** Optimum Moisture Content
- **PC –** Portland Cement
- **UoP-CEB machine –** University of Portsmouth Compressed Earth Block Machine
- **USCS –** Unified Soil Classicisation System

References:

[1] T. Bowen, A best practices manual for using compressed earth blocks in sustainable home construction in Indian country, (2017) 1–45. https://www.huduser.gov/portal/sites/default/files/pdf/Compressed-Earth-Blocks.pdf.

[2] H. Houben, H. Guillaud, Earth Construction A Comprehensive Guide, Intermediate Technology Publications, London, 1994.

[3] K. Park, D. Monitoring, T. Morton, F. Stevenson, B. Taylor, N.C. Smith, Low Cost Earth Brick Construction, Arc, Chartered Architects, Fife, 2005.

[4] D. Harper, Alternative Methods of Stabilisation for Unfired Mud Bricks, Newcastle University, 2011.

[5] R. El Nabouch, Q.-B. Bui, P. Perrotin, O. Plé, J.-P. Plassiard, Numerical modeling of rammed earth constructions: analysis and recommendations, First Int. Conf. Bio-Based Build. Mater. (2015) 21–24.

[6] M. Ben Mansour, E. Ogam, A. Jelidi, A.S. Cherif, S. Ben Jabrallah, Influence of compaction pressure on the mechanical and acoustic properties of compacted earth blocks: An inverse multi-parameter acoustic problem, Appl. Acoust. 125 (2017) 128–135. https://doi.org/10.1016/j.apacoust.2017.04.017.

[7] B. Little, T. Morton, Building with earth in Scotland: Innovative design and sustainability, (2001) 1–72. http://www.arc-architects.com/downloads/Buildng-With-Earth-in-Scotland-Report-2002.pdf%0Ahttps://www.webarchive.org.uk/wayback/archive/20170401194558/http://www.gov.scot/Publications/2002/02/10646/File-1.

[8] V. Rigassi, Compressed Earth Blocks: Manual of Production, Deutsches Zentrum für Entwicklungstechnologien, Deutsche Gesellschaft für Technische Zusammenarbeit, 1985.

[9] International Labour Office, United Nations Industrial Development Organization, Small-Scale Manufacture of Stabilised Soil Blocks, International Labour Office, Switzerland, 1987.

[10] H. Danso, B. Martinson, M. Ali, C. Mant, Performance characteristics of enhanced soil blocks: A quantitative review, Build. Res. Inf. 43 (2015) 253–262. https://doi.org/10.1080/09613218.2014.933293.

[11] A. Guettala, B. Mezghiche, R. Chebili, H. Houari, Durability of Lime Stablised Earth Blocks, Challenges Concr. Constr. Vol. 5, Sustain. Concr. Constr. (2002) 645–654. https://doi.org/10.1680/scc.31777.0064.

[12] P.P. Yalley, A.S.K. Kwan, Use of waste and low energy material in building block construction, Proc. 25th Conf. Passiv. Low Energy Archit. (PLEA 2008). (2008) 6.

[13] P. Turgut, B. Yesilata, Physico-mechanical and thermal performances of newly developed rubber-added bricks, Energy Build. 40 (2008) 679–688. https://doi.org/10.1016/j.enbuild.2007.05.002.

[14] British Standards Institute, BS EN 1996-1-1:2005+A1:2012, Eurocode 6. Des. Mason. Struct. Gen. Rules Reinf. Unreinforced Mason. Struct. (2005). https://bsol.bsigroup.com.

[15] A. Heath, D. Maskell, P. Walker, M. Lawrence, C. Fourie, Modern earth masonry: Structural properties and structural design., Struct. Eng. 90 (2012) 38–44.

[16] J.E. Oti, J.M. Kinuthia, Stabilised unfired clay bricks for environmental and sustainable use, Appl. Clay Sci. 58 (2012) 52–59. https://doi.org/10.1016/j.clay.2012.01.011.

[17] Linyi YLF Trading Company Limited, YLF1-40 manual interlocking brick machine, (2020). http://www.chinablockmachines.com/YLF1-40-manual-interlocking-brick-machine.html.

[18] P.J. Walker, Strength and erosion characteristics of earth blocks and earth block masonry, J. Mater. Civ. Eng. 16 (2004) 497–506. https://doi.org/10.1061/(ASCE)0899-1561(2004)16:5(414).

[19] V.G. Srisanthi, L. Keshav, P. Poorna Kumar, T. Jayakumar, Finite element and experimental analysis of 3D masonry compressed stabilised earth block and brick building models against earthquake forces, Period. Polytech. Civ. Eng. 58 (2014) 255–265. https://doi.org/10.3311/PPci.7443.

[20] H. Ben Ayed, O. Limam, M. Aidi, A. Jelidi, Experimental and numerical study of Interlocking Stabilized Earth Blocks mechanical behavior, J. Build. Eng. 7 (2016) 207–216. https://doi.org/10.1016/j.jobe.2016.06.012.

[21] S. Antony, A. Cherouat, G. Montay, Experimental, analytical and numerical analysis to investigate the tensile behaviour of hemp fibre yarns, Compos. Struct. 202 (2018) 482–490. https://doi.org/10.1016/j.compstruct.2018.02.074.

[22] J.D. Sitton, Y. Zeinali, W.H. Heidarian, B.A. Story, Effect of mix design on compressed earth block strength, Constr. Build. Mater. 158 (2018) 124–131. https://doi.org/10.1016/j.conbuildmat.2017.10.005.

[23] A. Pantano, B. Zuccarello, Numerical model for the characterization of biocomposites reinforced by sisal fibres, Procedia Struct. Integr. 8 (2018) 517–525. https://doi.org/10.1016/j.prostr.2017.12.051.

[24] F. Parisi, C. Balestrieri, H. Varum, Nonlinear finite element model for traditional adobe masonry, Constr. Build. Mater. 223 (2019) 450–462. https://doi.org/10.1016/j.conbuildmat.2019.07.001.

[25] D. Gooding, T. Thomas, Soilcrete blocks: Experimental work to determine whether cement or compaction pressure is more effective, Build. Res. Inf. 25 (1997) 202–209. https://doi.org/10.1080/096132197370327.

[26] D.J.T. Webb, Stabilised Soil Building Blocks., University of Newcastle Upon Tyne, Newcastle., 1988. http://hdl.handle.net/10443/283.

[27] Autodesk Inc, AutoCAD 2019, (2019). https://www.autodesk.com/education/free-software/autocad.

[28] Malvern Panalytical Ltd, Mastersizer 3000, (2020). https://www.malvernpanalytical.com/en/products/product-range/mastersizer-range?creative=328687395069&keyword=mastersizer&matchtype=e&network=g&device=c&gclid=EAIaIQobChMImbDMvZvv6AIVhbTtCh1YeAhXEAAYASAAEgLaCPD_BwE (accessed March 1, 2020).

[29] T. Morton, R. Bennetts, Earth Masonry, IHS BRE Press, Bracknell, 2008.

[30] British Standards Institute, BS 1377-2:1990, Methods Test Soils Civ. Eng. Purp. Classif. Tests . (1990). https://bsol.bsigroup.com.

[31] CreteAngle, Model “LE Standard Duty” Forced Action Pan Mixer, (2020). https://www.creteangle.com/products/model-le-standard-duty-forced-action-pan-mixer.

[32] Genlab Ltd, Genlab Classic Ovens, (2020). https://www.genlab.co.uk/57-genlab-classic-ovens (accessed June 10, 2020).

[33] British Standards Institute, BS EN 772-1:2011+A1:2015., Methods Test Mason. Units. Determ. Compressive Strength. (2011). https://bsol.bsigroup.com.

[34] Minitab Inc, Minitab 17.3.1, (2016). https://www.minitab.com/en-us/.

[35] ANSYS Incorporation, Workbench (Version 19.1 Academic Teaching Introductory), (2019).

[36] J.I. Gisbert, D. Bru, A. Gonzalez, S. Ivorra, Masonry micromodels using high order 3D elements, Procedia Struct. Integr. 11 (2018) 428–435. https://doi.org/10.1016/j.prostr.2018.11.055.

[37] M. Klabník, J. Králik, Equivalent Stress and Strain of Composite Column under Fire, Procedia Eng. 190 (2017) 522–529. https://doi.org/10.1016/j.proeng.2017.05.374.

[38] R. Khajehdehi, N. Panahshahi, Effect of openings on in-plane structural behavior of reinforced concrete floor slabs, J. Build. Eng. 7 (2016) 1–11. https://doi.org/10.1016/j.jobe.2016.04.011.

[39] N. Lahmar, F. Bouziadi, B. Boulekbache, E. Meziane, M. Hamrat, Experimental and finite element analysis of shrinkage of concrete made with recycled coarse aggregates subjected to thermal loading, Constr. Build. Mater. 247 (2020) 118564. https://doi.org/10.1016/j.conbuildmat.2020.118564.

[40] M. Martínez, S. Atamturktur, Experimental and numerical evaluation of reinforced dry-stacked concrete masonry walls, J. Build. Eng. 22 (2019) 181–191. https://doi.org/10.1016/j.jobe.2018.12.007.

[41] A.C. Aydin, S.G. Özkaya, The finite element analysis of collapse loads of single-spanned historic masonry arch bridges (Ordu, Sarpdere Bridge), Eng. Fail. Anal. 84 (2018) 131–138. https://doi.org/10.1016/j.engfailanal.2017.11.002.

[42] P.K. Mehta, J.. P. Monteiro, Concrete: Microstructure, Properties, and Materials, Fourth Edi, McGraw-Hill Education, 2014.

[43] J. Morel, A. Pkla, A model to measure compressive strength of compressed earth blocks, Constr. Build. Mater. 16 (2002) 303–310.

[44] A. Heath, D. Maskell, P. Walker, M. Lawrence, C. Fourie, Modern earth masonry - Structural properties & structural design, Struct. Eng. 90 (2012) 38–44.

[45] L. Miccoli, A. Garofano, P. Fontana, U. Müller, Experimental testing and finite element modelling of earth block masonry, Eng. Struct. 104 (2015) 80–94. https://doi.org/10.1016/j.engstruct.2015.09.020.

[46] H. Smoljanović, N. Živaljić, Ž. Nikolić, A. Munjiza, Numerical analysis of 3D dry-stone masonry structures by combined finite-discrete element method, Int. J. Solids Struct. 136–137 (2018) 150–167. https://doi.org/10.1016/j.ijsolstr.2017.12.012.